Surface and guided-wave polariton modes of magnetoplasma films in the Voigt geometry

1994 J. Phys.: Condens. Matter 6 4233

(http://iopscience.iop.org/0953-8984/6/23/003)

J. Phys.: Condens. Matter 6 (1994) 4233–4246. Printed in the UK

Surface and guided-wave polariton modes of magnetoplasma films in the Voigt geometry

F G Elmzughi†‡ and D R Tilley†§

† Department of Physics, University of Essex, Colchester CO4 3SQ, UK
‡ Physics Department, Al-Fatah University, Post Box 13540, Tripoli, Libya

Received 3 March 1994

Abstract. We discuss retarded electromagnetic modes of a film containing one or two species of carriers in the presence of an in-plane magnetic field. It is assumed that the film is characterized by a gyrodielectric tensor containing cyclotron and plasma response. We deal with the Voigt geometry (propagation transverse to the field) for both a symmetric film and a film on a substrate. A detailed discussion is given of the guided-wave modes that occupy the bulk continuum region. For the symmetric film, dispersion curves of both surface-type and guided-wave modes are reciprocal, $\omega(-q) = \omega(q)$, but field profiles are different for $+q$ and $-q$. For the film on a substrate both the dispersion curves and the field profiles are non-reciprocal. Numerical illustrations are given for the parameters of CMT, $Cd_{1-x}Hg_xTe$.

1. Introduction

The far-infrared properties of doped semiconductors in the presence of a magnetic field H_0 show a number of features additional to those found in the absence of a field. The propagation of surface modes is non-reciprocal [1], which means that the frequency changes when the direction of travel is reversed. A similar property holds for oblique-incidence reflectivity. Non-reciprocity arises from the gyrotropic form of the dielectric tensor, that is, the presence of non-zero off-diagonal terms proportional to H_0. Since these terms arise ultimately from the Lorentz force, they have different signs for electrons and holes. Consequently magnetoplasma reflectivity can be used in principle to determine the parameters of both species of carriers in counter-doped semiconductors [2].

In [2] the effect of the presence of two species of carrier was illustrated with calculations of normal-incidence reflectivity. Some calculations for oblique incidence have been presented recently [3]. Here we turn to the surface-polariton and related modes that propagate in a magnetoplasma thin film. A substantial account for the one-component magnetoplasma has already been given by Kushwaha and Halevi [4–6]. In these papers they dealt with the Faraday geometry (H_0 in the plane of the film and propagation along H_0) [4], the Voigt geometry (H_0 in the plane and propagation normal to H_0) [5] and the perpendicular geometry (H_0 normal to the plane) [6]. A further paper [7] deals with the interaction between the magnetoplasma polaritons and an optic phonon in the substrate. In addition to considering the effects of having two components we go beyond the previous work by including a full discussion of guided-wave modes, which can be important in experimental spectra [8]. We restrict our attention to the Voigt geometry.

§ From 1st October 1994: School of Physics, Universiti Sains Malaysia, 11800 USM, Penang, Malaysia.

0953-8984/94/234233+14$19.50

The bulk dispersion equation is important since it defines the 'windows' in the frequency–wavevector plane in which surface and guided waves are found. The bulk equation is therefore discussed briefly in section 2. Surface-polariton modes propagate on the interface between the magnetoplasma and vacuum in parts of the frequency intervals that form stop bands for the bulk modes. In a film, surface-like modes propagate in the same frequency intervals. If the film is not too thin they can be seen as arising from the surface polaritons on the semi-infinite medium with a frequency splitting due to perturbation by the second interface of the film. For this reason, section 2 also contains a discussion of the surface modes on a semi-infinite medium. The dispersion equation for the film is derived in section 3. The same equation describes both surface-like and guided modes; their properties are discussed in a unified manner in sections 3 to 5. Conclusions are presented in section 6. For numerical illustrations we use parameters appropriate for good-quality $Hg_xCd_{1-x}Te$ (CMT) with $x = 0.22$ at room temperature. These are [9] electron effective mass $m_e^* = 0.013m_e$, hole effective mass $m_h^* = 0.4m_e$ and high-frequency dielectric constant $\epsilon = 13.5$. These give plasma frequencies $\omega_{pe}/2\pi c = 84.2\ cm^{-1}$ and $\omega_{ph}/2\pi c = 17.1\ cm^{-1}$ with cyclotron resonance frequencies $\omega_{ce}/2\pi c = 71.8B_0\ cm^{-1}$ and $\omega_{ch} = 2.397B_0\ cm^{-1}$ where B_0 is the magnetic field in tesla.

2. Bulk and surface modes

In the presence of a magnetic field B_0 along the z axis the dielectric tensor takes the form

$$\epsilon(\omega) = \begin{pmatrix} \epsilon_1 & -i\epsilon_2 & 0 \\ i\epsilon_2 & \epsilon_1 & 0 \\ 0 & 0 & \epsilon_3 \end{pmatrix} \tag{1}$$

where for a two-component system

$$\epsilon_1 = \epsilon_\infty + \sum_n \frac{\rho_n \omega_{Tn}^2}{\omega_{Tn}^2 - \omega^2 - i\omega\Gamma_n} + \sum_k \frac{\epsilon_\infty \omega_{pk}^2 (\omega - i/\tau_k)}{\omega(\omega_{ck}^2 - (\omega + i/\tau_k)^2)} \tag{2}$$

$$\epsilon_2 = \epsilon_\infty \sum_k \frac{\omega_{ck}\omega_{pk}^2}{\omega(\omega_{ck}^2 - (\omega + i/\tau_k)^2)} \tag{3}$$

and

$$\epsilon_3 = \epsilon_\infty + \sum_n \frac{\rho_n \omega_{Tn}^2}{\omega_{Tn}^2 - \omega^2 - i\omega\Gamma_n} - \sum_k \frac{\epsilon_\infty \omega_{pk}^2}{\omega(\omega + i/\tau_k)}. \tag{4}$$

The sums over n represent different optic-phonon contributions with TO frequencies ω_{Tn}, dipole strengths ρ_n and dampings Γ_n. The sums over k represent free-carrier contributions with cyclotron frequencies $\omega_{ck} = eB_0/m_k$, plasma frequencies $\omega_{pk} = n_k e^2/\epsilon_0 m_k$ and lifetimes τ_k. Here n_k and m_k are the density and effective mass of the carriers of species k. For the two-component case k = e or h, electrons or holes. In the absence of damping ϵ_1 and ϵ_2 are both real so ϵ is Hermitian. It is seen that both ϵ_1 and ϵ_2 have poles at the cyclotron resonance frequencies ω_{ce} and ω_{ch}; in effect the magnetic field lifts the plasma pole above zero frequency. Equation (1) includes contributions from optically active phonons since such phonons occur in many semiconductors that support magnetoplasmas. For the sake of

clarity in numerical illustrations we omit this term; this is realistic for cases when ω_T and the cyclotron frequencies are well separated. Although damping terms are included in the above equations we drop them for the discussion of dispersion equations since the resulting graphs contain the essential information for planning and interpretation of experiments.

The usual derivation shows that a bulk mode propagating transverse to B_0 has dispersion relation

$$q_x^2 + q_y^2 = \epsilon_V \omega^2/c^2 \tag{5}$$

where

$$\epsilon_V = \epsilon_1 - \epsilon_2^2/\epsilon_1 \tag{6}$$

is the Voigt permittivity. The frequency dependence of ϵ_V for various cases is illustrated in [2]. As mentioned, (5) defines the windows for surface and guided-wave propagation and it will be discusses as such subsequently.

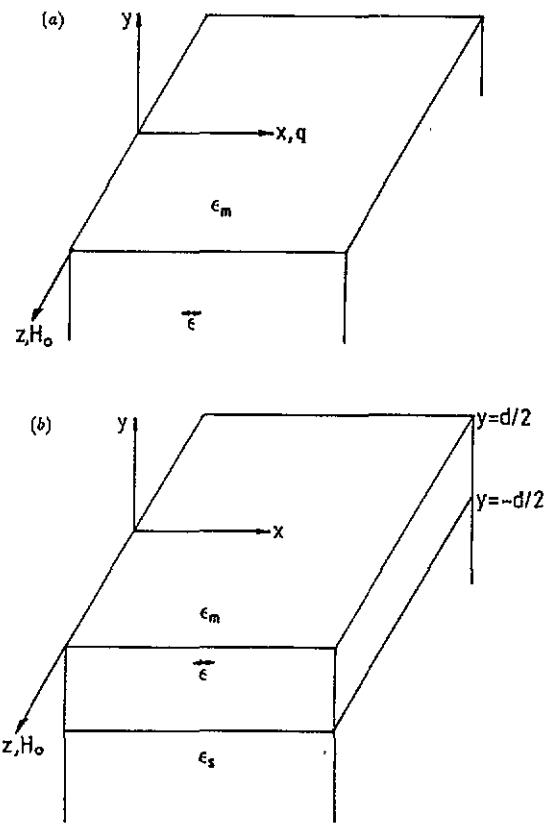

Figure 1. Geometries and choices of axes for Voigt propagation: (a) surface; (b) film on substrate.

We consider next the interface between the magnetoplasma and a region with frequency-independent dielectric constant ϵ_m; as shown in figure 1(a) the y axis is chosen as the

normal to the interface with x as the propagation direction of the surface polariton. The derivation of the surface-mode dispersion relation [10] involves finding the condition for the wave $\exp(iq_x x - i\omega t)$ to be a solution of Maxwell's equations and the interface boundary conditions. Since the bulk equations apply in either medium, then if the y dependence is taken as $\exp(iq_y y)$ (5) applies in the lower medium with the similar

$$q_x^2 + q_y^2 = \epsilon_m \omega^2/c^2 \tag{7}$$

for the upper medium. The surface polariton is localized at the interface so that in both media q_y must be imaginary, $q_y = -i\alpha$ in the lower medium and $q_y = i\alpha'$ in the upper medium. The signs ensure convergence at $-\infty$ and $+\infty$ respectively. In view of (5) and (7) the definitions of α and α' are

$$\alpha = (q_x^2 - \epsilon_V \omega^2/c^2)^{1/2} \tag{8}$$

$$\alpha' = (q_x^2 - \epsilon_m \omega^2/c^2)^{1/2}. \tag{9}$$

Clearly the inequalities

$$q_x^2 > \epsilon_V \omega^2/c^2 \tag{10}$$

and

$$q_x^2 > \epsilon_m \omega^2/c^2 \tag{11}$$

are required.

The surface polariton is p polarized (H field transverse) and the conditions that E_x and H_y should be continuous at the interface lead to the dispersion relation

$$\alpha + \alpha' \epsilon_V - q_x(\epsilon_2/\epsilon_1) = 0. \tag{12}$$

The most striking property of (12) is that the third term is linear in q_x, so the dispersion graph $\omega(q_x)$ is indeed non-reciprocal, $\omega(-q_x) = \omega(q_x)$.

Equations (10) and (11) define the regions of the ω–q_x plane in which solutions of (12) are to be sought. The results hold for any form of ϵ_m but for illustration we consider only a vacuum interface, $\epsilon_m = 1$. Equation (11) then requires that q_x lie to the right of the vacuum light line. Graphs for the one- and two-component cases are shown in figure 2(a) and 2(b) respectively. Since the abcissa in figure 2 is q_x, (5) defines the continuum $q_x^2 < \epsilon_V \omega^2/c^2$ throughout which bulk modes can propagate with some value of q_y. The number of bulk continuum regions is governed by the number of poles of ϵ_V since $q_x \to \infty$ on the positive side of the pole and there is no solution for q_x on the negative side of the pole. As is apparent from the expressions for ϵ_1 and ϵ_2 in (2) and (3) ϵ_V has one more pole for the two-component than for the one-component case and there are therefore three continua for the two-component case compared with two for the one-component case. The stop bands of the bulk modes are the surface-mode windows; there are therefore two in figure 2(a) and three in figure 2(b). The non-reciprocity, that is, the difference between $+q_x$ and $-q_x$ modes, is clearly seen in figure 2(a) and 2(b). In fact, in the lower window in figure 2(a) the + mode is a 'real' mode persisting to $q_x \to \infty$ but the − mode is 'virtual', terminating at a finite value of q_x in the bulk continuum. The situation is reversed in the upper window. Similar comments apply to the three surface-mode windows in figure 2(b).

The main difference between figure 2(a) and 2(b) is the appearance of a very low-frequency window in the latter. The frequency is low simply because of the small value of ω_{ch}. There are minor differences between the curves in the higher windows in the figures but not at a level that is likely to be significant for experiment.

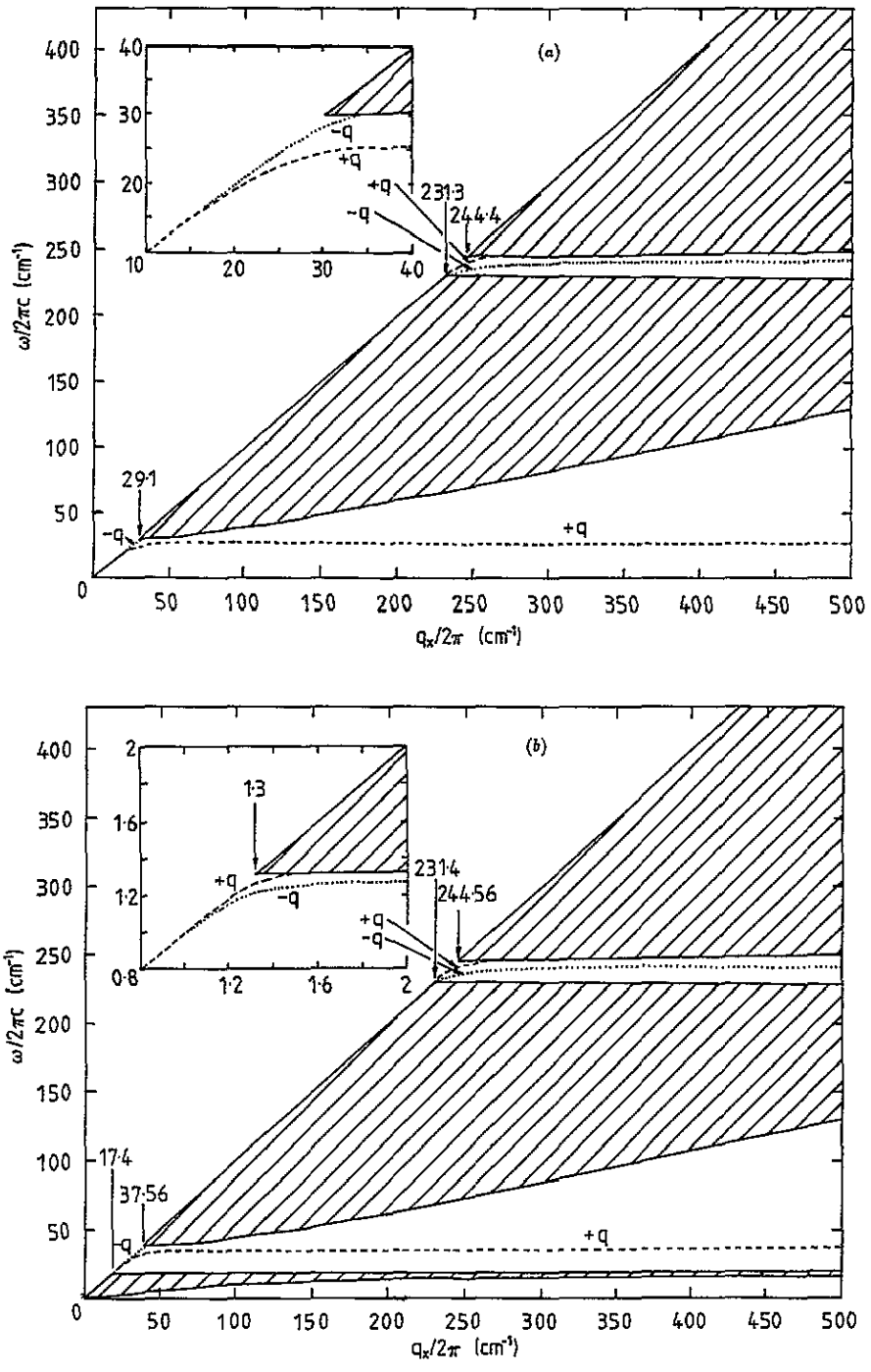

Figure 2. Surface-polariton dispersion curves for (a) a one-component (electrons) and (b) a two-component (electrons plus holes) magnetoplasma in a field $B_0 = 3$ T: dashed lines, $+q_x$ surface modes; dotted lines, $-q_x$ surface modes. The bulk continuum regions are shown shaded and relevant bounding frequencies are marked. The insets show the lowest-frequency surface-mode region in each case.

3. Film modes: formalism

We take the geometry shown in figure 1(b): a magnetoplasma film is deposited on a substrate with scalar dielectric constant ϵ_s and the medium above the film has scalar dielectric constant ϵ_m. Maxwell's equations are to be solved together with boundary conditions at each interface. Equations (5) and (7) apply in each medium. It is clear from the form of ϵ in (1) that the more interesting case is p polarization, since the E field is in the x–y plane, so the components E_x and E_y are coupled by the off-diagonal terms in (1). The field components in the three media can be written

$$\boldsymbol{E} = (E_{1x}, -(q_x/q_{1y})E_1\hat{x}, 0)\exp(\mathrm{i}q_{1y}y)\exp\mathrm{i}(q_x x - \omega t) \qquad y > 0 \tag{13}$$

$$\begin{aligned}\boldsymbol{E} = \left\{a\exp\left(\mathrm{i}q_{2y}\left(y+\frac{d}{2}\right)\right) + b\exp\left(-\mathrm{i}q_{2y}\left(y+\frac{d}{2}\right)\right), -\frac{\epsilon_1 q_x - \mathrm{i}\epsilon_2 q_{2y}}{\mathrm{i}\epsilon_2 q_x + \epsilon_1 q_{2y}}a\right.\\ \times\exp\mathrm{i}q_{2y}\left(y+\frac{d}{2}\right) - \frac{\epsilon_1 q_x + \mathrm{i}\epsilon_2 q_{2y}}{\mathrm{i}\epsilon_2 q_x - \epsilon_1 q_{2y}}b\exp\left(-\mathrm{i}q_{2y}\left(y+\frac{d}{2}\right)\right), 0\Big\}\\ \times\exp\mathrm{i}(q_x x - \omega t) \qquad 0 > y > -d\end{aligned} \tag{14}$$

$$\boldsymbol{E} = (E_{3x}, -(q_x/q_{3y})E_{3x}, 0)\exp(\mathrm{i}q_{3y}(y+d))\exp\mathrm{i}(q_x x - \omega t). \qquad y < -d. \tag{15}$$

Here q_{1y} and q_{3y} must be purely imaginary to ensure boundedness at infinity, explicitly $q_{1y} = \mathrm{i}\alpha_1$ and $q_{3y} = -\mathrm{i}\alpha_3$. The inverse penetration lengths α_1 and α_3 are given by relations like (9). In contrast to the single-surface case, however, q_{2y} can be either purely imaginary or purely real. The former corresponds to surface-type modes in regions of the ω–q_x plane where (10) is satisfied whereas the latter correspond to guided-wave modes within the bulk continuum regions shown in figure 2, that is in regions satisfying

$$q_x^2 < \epsilon_V\omega^2/c^2. \tag{16}$$

The two boundary conditions at each interface give four homogeneous equations for the four coefficients E_{1x}, a, b and E_{3x}; the solvability condition is the dispersion equation. This can be written in the form

$$\begin{aligned}&\frac{\epsilon_1 q_{1y}(\epsilon_1 q_x + \mathrm{i}\epsilon_2 q_{2y}) + (\mathrm{i}\epsilon_2 q_{2y} - \epsilon_g q_x)(\mathrm{i}\epsilon_2 q_x - \epsilon_1 q_{2y})}{\epsilon_1 q_{1y}(\epsilon_1 q_x - \mathrm{i}\epsilon_2 q_{2y}) + (\mathrm{i}\epsilon_2 q_{1y} - \epsilon_g q_x)(\mathrm{i}\epsilon_2 q_x + \epsilon_1 q_{2y})}\exp(-\mathrm{i}q_{2y}d)\\ &\quad= \frac{\epsilon_1 q_{3y}(\epsilon_1 q_x + \mathrm{i}\epsilon_2 q_{2y}) + (\mathrm{i}\epsilon_2 q_{3y} - \epsilon_s q_x)(\mathrm{i}\epsilon_2 q_x - \epsilon_1 q_{2y})}{\epsilon_1 q_{3y}(\epsilon_1 q_x - \mathrm{i}\epsilon_2 q_{2y}) + (\mathrm{i}\epsilon_2 q_{3y} - \epsilon_s q_x)(\mathrm{i}\epsilon_2 q_x + \epsilon_1 q_{2y})}\exp(\mathrm{i}q_{2y}d)\end{aligned} \tag{17}$$

which reduces to

$$[q_{1y}q_{3y}(\epsilon_1^2 - \epsilon_2^2) + k^2\epsilon_s\epsilon_g - \mathrm{i}\epsilon_2 q_x(q_{3y}\epsilon_g + q_{1y}\epsilon_s)]\tanh(\mathrm{i}q_{2y}d) + \epsilon_1 q_{2y}(q_{1y}\epsilon_s - q_{3y}\epsilon_g) = 0 \tag{18}$$

where $k^2 = q_x^2 - \omega^2/c^2$. This can be seen to be the same as the corresponding equation in [5]. For the particular case of a symmetric configuration, $\epsilon_m = \epsilon_s$, (18) divides into solutions in which E_x is either even or odd about the mid-point of the film with the two dispersion equations

$$(\alpha_1\epsilon_V)^2 + (\epsilon\alpha_2)^2 - ((\epsilon\epsilon_2/\epsilon_1)q_x)^2 = -2\epsilon\epsilon_V\alpha_1\alpha_2\tanh(\alpha_2 d) \tag{19}$$

and

$$(\alpha_1\epsilon_V)^2 + (\epsilon\alpha_2)^2 - ((\epsilon\epsilon_2/\epsilon_1)q_x)^2 = -2\epsilon\epsilon_V\alpha_1\alpha_2\coth(\alpha_2 d) \tag{20}$$

where $\epsilon_s = \epsilon_g = \epsilon$. Equations (19) and (20) are written in terms of α_2 defined by $q_{2y} = \mathrm{i}\alpha_2$; they could equally be written in terms of q_{2y} since as remarked q_{2y} can be either real (guided waves) or imaginary (surface-type waves).

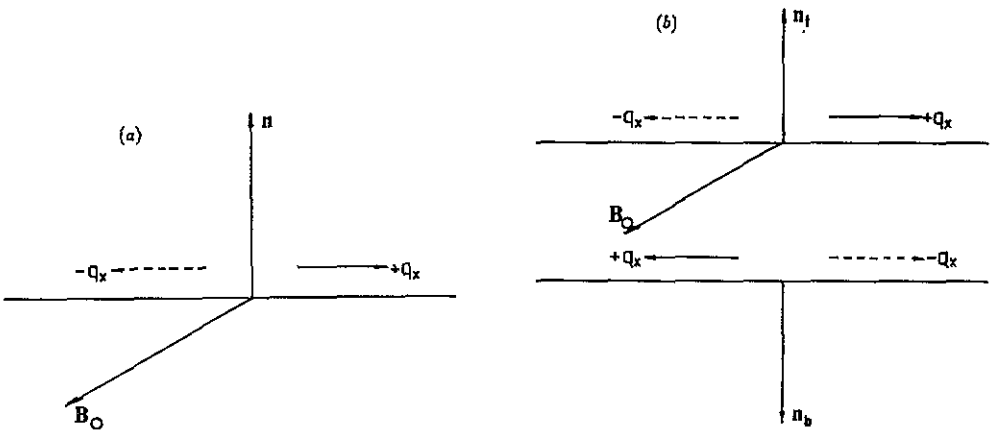

Figure 3. A sketch of surface-mode propagation for (a) a single interface and (b) a thick film. Modes marked $+q_x$ all have the same frequency, as do modes marked $-q_x$. Localization is indicated by the positioning of the arrows.

4. Symmetric films

We start by discussing the surface-type modes of the symmetric film, (19) and (20) with α_2 real. It may be noted that these describe reciprocal propagation since q_x occurs only as q_x^2. The reason can be seen from figure 3. As shown in figure 3(a), $+q_x$ in figure 2 is defined as the direction $n \times B_0$, where n is the normal to the surface. In figure 3(b) we indicate the mode frequencies for a thick film in which the modes on the two surfaces are effectively decoupled. Since the surface normals are in opposite directions the modes that propagate in the positive x direction are $+q_x$ on the upper surface but $-q_x$ on the lower surface. Thus both frequencies occur for either direction of propagation. The detailed form of the solutions depends on the value of film thickness d. For large d the hyperbolic functions may be replaced by unity and both equations read

$$(\alpha_1\epsilon_v + \alpha_2\epsilon_m)^2 - ((\epsilon_m\epsilon_2/\epsilon_1)q_x)^2 = 0. \tag{21}$$

This is just the product of the $+q_x$ and $-q_x$ forms of (12) so that in this thick limit (19) and (20) describe the plus and minus modes on the top and bottom surfaces. This is as depicted in figure 3. As d decreases the field profile of a top-surface mode, for example, reaches the lower interface so the dispersion curve is perturbed from the single-interface form. The dispersion curves of the surface modes for a one-component magnetoplasma are shown in figure 4 for a 10 μm film in a field of 3 T. The curves are seen to be similar to those for a single interface (figure 2(a)). However, they are not now marked as + and $-q_x$ modes since as illustrated in figure 3 both curves are found with either sign of q_x. The regions marked as bulk continua in figure 2(a) now have the significance of guided-wave windows. For the thickness chosen for figure 4 the upper mode in each surface-wave window is virtual while the lower is real, as for the single interface. For thin films, however, our numerical calculations show that both modes are real. For the two-component magnetoplasma the relation of the surface-type modes of a film to those for a single interface is similar and therefore no dispersion curves are shown.

Although the dispersion curves are reciprocal, the localization of the modes is not. This can be seen from the field profiles for the surface-wave modes. The field profile may be

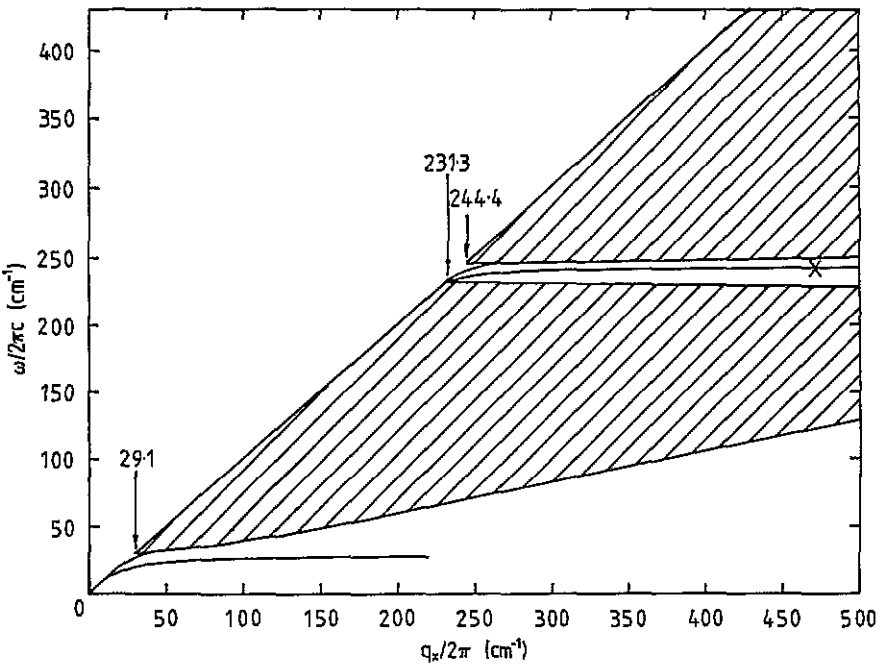

Figure 4. Surface-type polariton dispersion curves for a one-component magnetoplasma symmetric thin film of thickness $d = 10$ μm with bounding medium $\epsilon_m = 1$ (vacuum) in a field of 3 T. The guided-wave windows are shown shaded.

defined as the dependence on y of the quantity $\mathrm{Re}(E_{2x}/E_{1x})$ where E_{2x} is defined in (14). When ω and q_x are on the dispersion curve (13) and (14) can be solved for the ratios a/E_{1x} and b/E_{1x} so that the field profile can then be drawn. An example is shown in figure 5 for the $+q_x$ and $-q_x$ modes at the point marked X in figure 4. As can be seen, in agreement with figure 3 the $+q_x$ mode is localized at $y = -d/2$ while the $-q_x$ mode is localized at $y = +d/2$.

The guided-wave modes of the symmetric film are the solutions of (19) and (20) with q_{2y} real. They occur in the windows defined by (16) together with (11), that is, the regions that were marked as bulk continua in figures 2 and 4. For the same reason as the surface-type modes the dispersion curves are reciprocal but the field profiles are not. Examples of dispersion curves are shown in figure 6. There are two windows for the one-component case and three for the two-component case. The guided-mode dispersion curves occur in pairs originating on the light line (7); one of the pair has even and the other odd symmetry about the mid-point of the film. For the one-component magnetoplasma, figure (6(a) and 6(b), all the curves in the lower window have a common asymptote for $q_x \to \infty$, namely the frequency at which ϵ_y has a pole. The spacing of the modes depends on the value of d and as with conventional guided modes the dispersion curves are more closely spaced for the larger value of d. This can be seen in the comparison between figure 6(a) and 6(b). For the two-component magnetoplasma, figure 6(c) and 6(d), the curves in each of the two lower windows all have as asymptopic frequency one of the two poles of ϵ_y. Again, comparison of figure 6(d) with 6(c) shows the characteristic closer spacing of the curves for the thicker film.

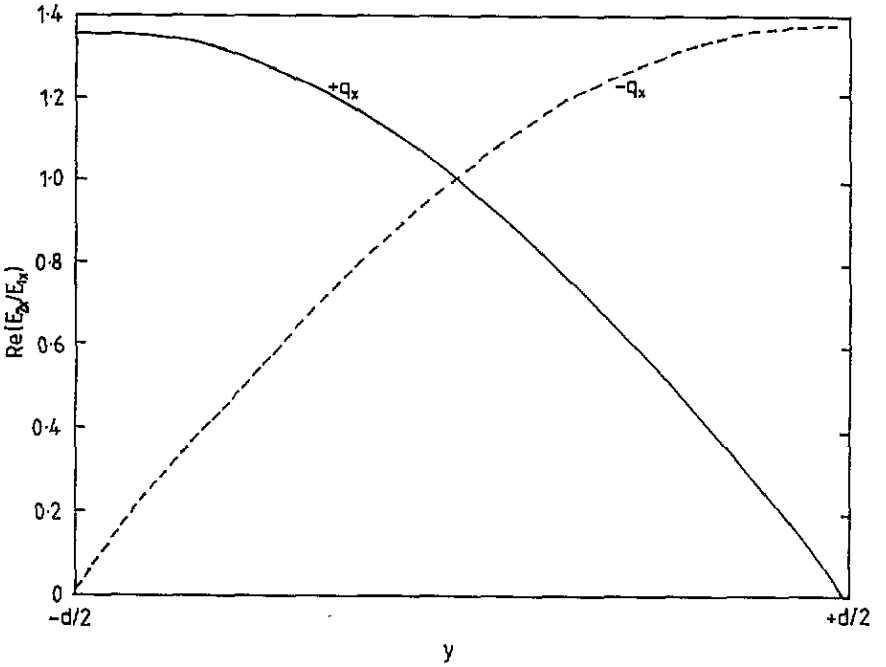

Figure 5. The field profiles for $+q_x$ (solid line) and $-q_x$ (dashed line) surface modes of a symmetric one-component film. These are drawn for the point $\omega/2\pi c = 242$ cm^{-1}, $q_x/2\pi = 472$ cm^{-1} marked on the upper real dispersion curve in figure 4.

5. Asymmetric films

We now turn to the more practical case of a film on a substrate for which some differences are seen in the dispersion curves compared with the symmetric case. In particular, the dispersion is non-reciprocal. As seen in figure 5, even in a symmetric film although propagation is reciprocal the field profiles are different for the $+q_x$ and $-q_x$ modes. When the dielectric constants of the bounding media are not the same this difference leads to non-reciprocity of the dispersion. A second property is that in the asymmetric case the modes no longer have a definite parity about the mid-point of the film.

The surface-type modes of a one-component asymmetric film are illustrated in figure 7. The dispersion curves occupy essentially the same windows as those for the modes on a single surface, figure 2(a). The non-reciprocity can be seen in the comparison between figure 7(a) and 7(b), particularly in the upper window. By comparison with figure 4 it is seen that the introduction of the substrate removes both virtual modes for $-q_x$ propagation and the lower virtual mode for $+q_x$ propagation.

Guided-wave modes for the same film are shown in figure 8 for the case of $+q_x$ propagation. Examination of the data files for $+q_x$ and $-q_x$ shows that propagation is non-reciprocal but the differences are too small to show up clearly on a graph.

We do not show graphs for the two-component film on a substrate since the changes from the symmetric case are in line with those pointed out for the one-component case.

6. Conclusions

We have given a fuller discussion than has previously appeared of the surface and guided-

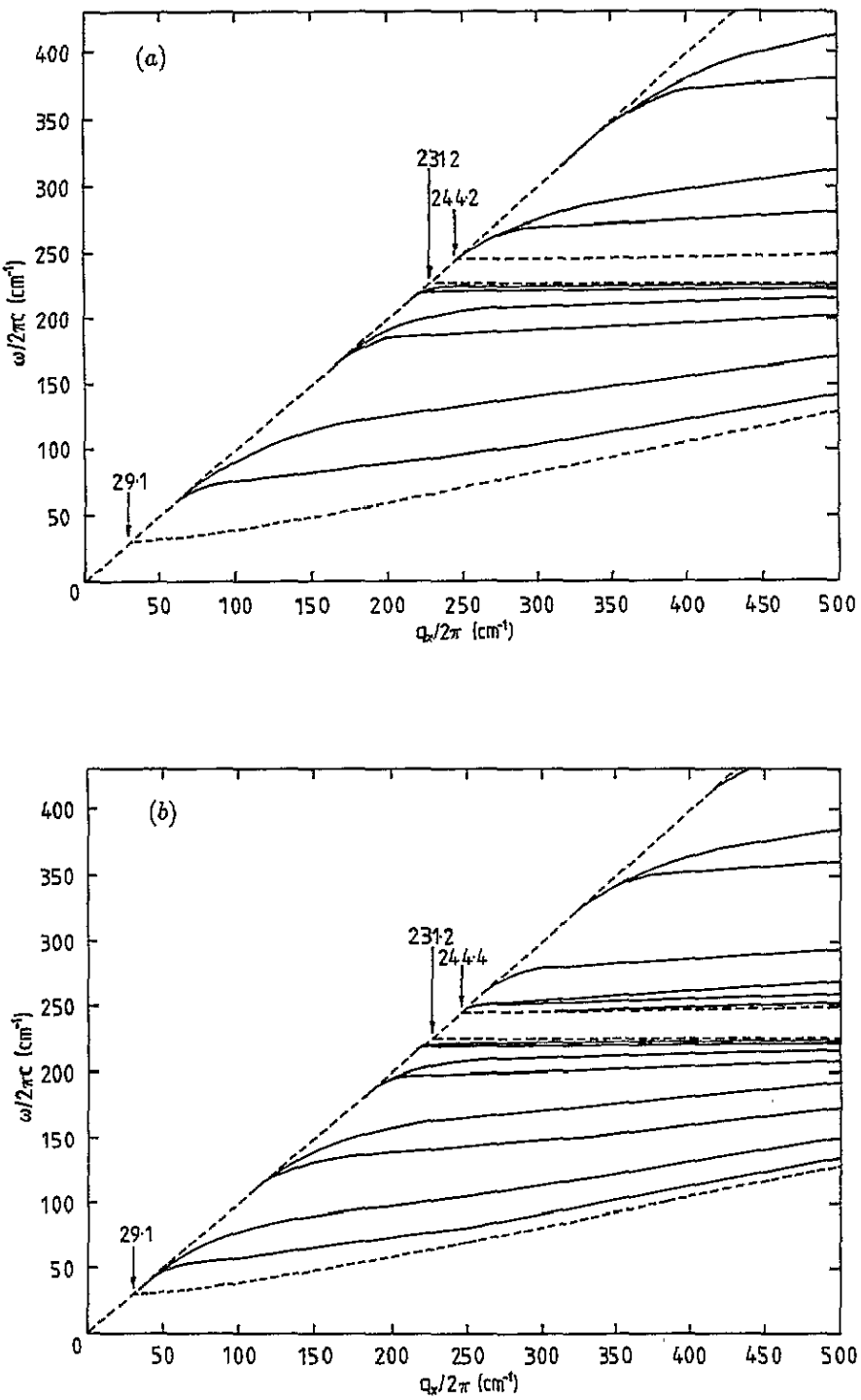

Figure 6. Guided-wave dispersion curves for symmetric one- and two-component films with bounding medium $\epsilon_m = 1$ (vacuum) in a field of 3 T: (a) one component, $d = 10$ μm; (b) one component, $d = 15$ μm; (c) two component, $d = 10$ μm, (d) two component, $d = 15$ μm. The boundaries of the guided-wave windows are shown dashed and the dispersion curves solid.

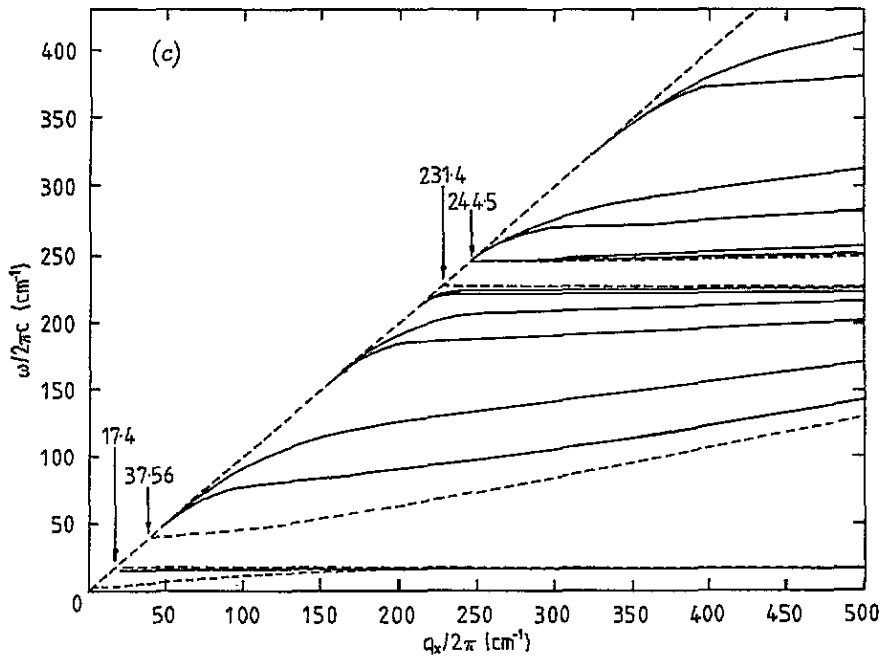

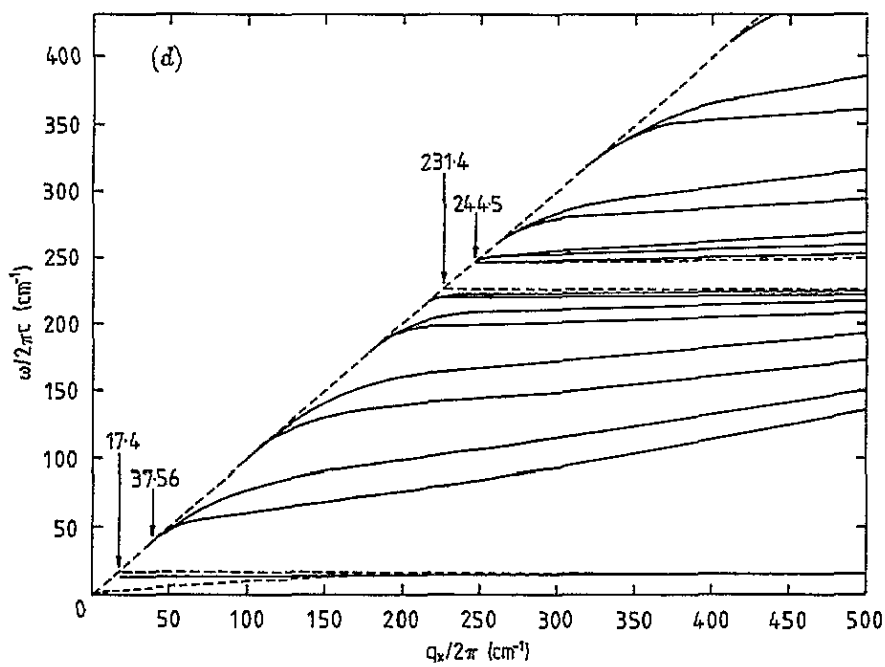

Figure 6. (Continued)

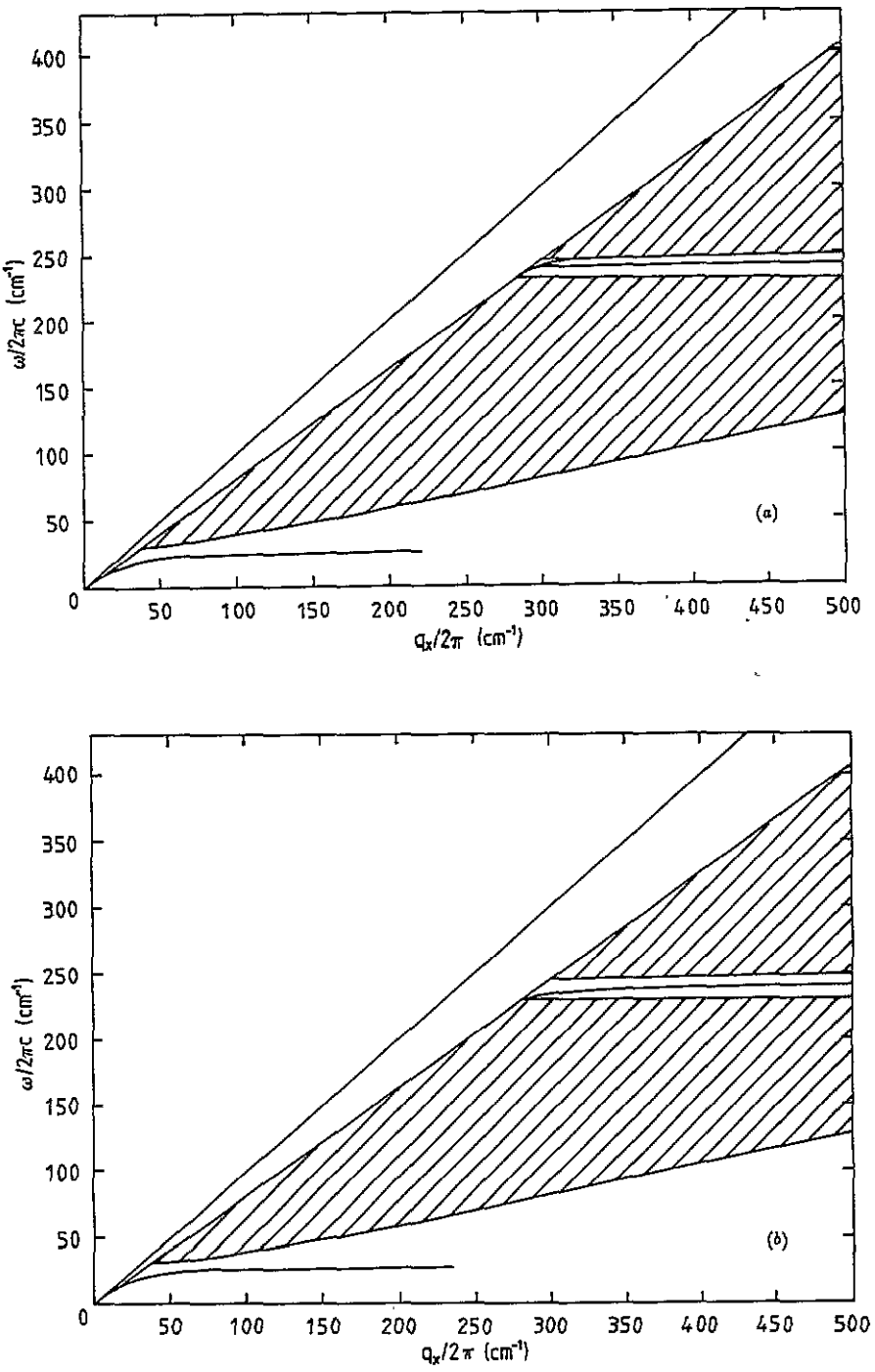

Figure 7. *Surface-type polariton dispersion curves for a one-component magnetoplasma film of* thickness $d = 10$ μm in a field of 3 T. The bounding media have $\epsilon_m = 1$ and $\epsilon_s = 1.5$. The light lines $q_x = \omega/c$ and $q_x = \epsilon_s^{1/2}\omega/c$ are drawn and the guided-wave windows are shown shaded. (a) $+q_x$ propagation; (b) $-q_x$ propagation.

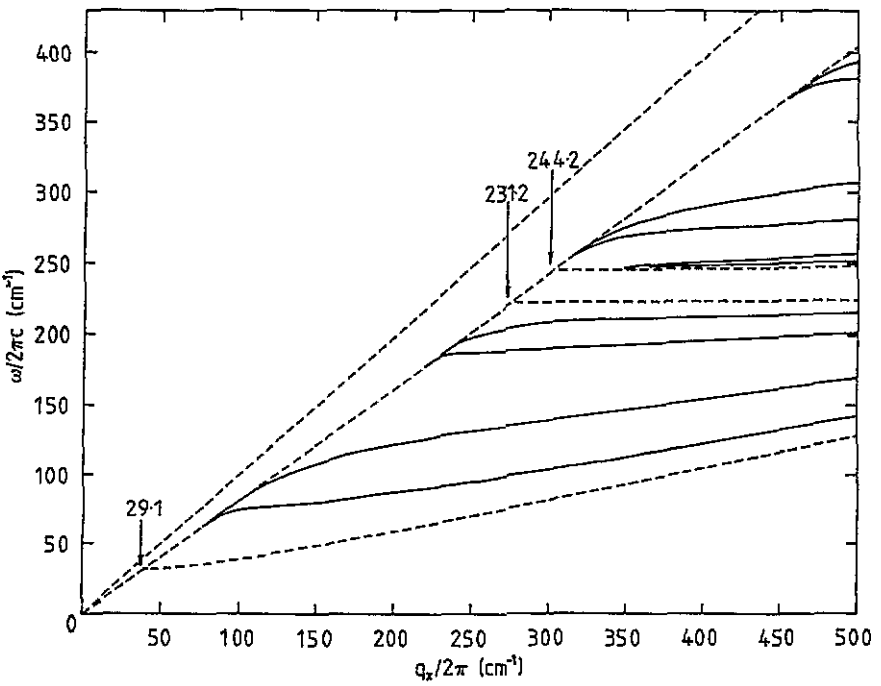

Figure 8. Guided-wave dispersion curves ($+q_x$ propagation) for a one-component magnetoplasma film of thickness $d = 10$ μm in a field of 3 T. The bounding media have $\epsilon_m = 1$ and $\epsilon_s = 1.5$; the corresponding light lines are shown. The boundaries of the guided-wave windows and the light lines are shown dashed and the dispersion curves solid.

wave modes of a magnetoplasma thin film together with an account of the differences between one- and two-component magnetoplasmas. For simplicity the effects of optically active phonons were excluded from the numerical illustrations although they are included in the formal expressions if the full form of the dielectric tensor is inserted. For the parameters of CMT the main effect of including the hole terms in ϵ is to introduce a low-frequency guided-wave window and associated third surface-mode region. In addition, detailed differences can be seen in the dispersion curves in other regions.

The most obvious technique to probe the magnetoplasma modes discussed here is attenuated total reflection (ATR), in which a far-infrared beam is incident through a prism of dielectric constant ϵ_p at an angle θ greater than the critical value $\theta_c = \sin^{-1}(\epsilon_p^{-1/2})$ for total internal reflection. The prism is spaced from the sample by a gap d. An ATR frequency scan probes the dispersion curves along the line $q_x = \epsilon_p^{1/2} \sin\theta(\omega/c)$ and a dip in the reflectivity is seen at each crossing point [8]. Calculation of an ATR spectrum involves straightforward development of a reflectivity program [3] so results have not been shown. The crucial parameter for resolution of modes by ATR is the magnitude of the damping parameters.

Acknowledgments

We are grateful for helpful discussions with Kamsul Abraha, Doug Brown, Tom Dumelow and Terry Parker. F G Elmzughi acknowledges support by Al-Fatah University.

References

[1] Camley R E 1987 *Surf. Sci. Rep.* **7** 103
[2] Johnson B L, Camley R E and Tilley D R 1991 *Phys. Rev.* B **44** 8837
[3] Elmzughi F and Tilley D R 1993 *18th Int. Conf. on Infrared and Millimeter Waves* ed J R Birch and T J Parker; *Proc. SPIE* **2104** 627
[4] Kushwaha M S and Halevi P 1987 *Phys. Rev.* B **35** 3879
[5] Kushwaha M S and Halevi P 1987 *Phys. Rev.* B **36** 5960
[6] Kushwaha M S and Halevi P 1988 *Phys. Rev.* B **38** 12428
[7] Kushwaha M S and Halevi P 1987 *Solid State Commun.* **64** 1405
[8] Dumelow T, Parker T J, Smith S R P and Tilley D R 1993 *Surf. Sci. Rep.* **17** 151
[9] Brown D E 1993 private communication
[10] Cottam M G and Tilley 1989 *Introduction to Surface and Superlattice Excitations* (Cambridge: Cambridge University Press)